Human Molecular Genetics, 2013, Vol. 22, No. 15 **2975–2983**
doi:10.1093/hmg/ddt149
Advance Access published on April 4, 2013

Deficiency of the E3 ubiquitin ligase TRIM2 in early-onset axonal neuropathy

Emil Ylikallio[1], Rosanna Pöyhönen[1], Magdalena Zimon[4,5], Els De Vriendt[4,5], Taru Hilander[1], Anders Paetau[2], Albena Jordanova[4,5], Tuula Lönnqvist[6] and Henna Tyynismaa[1,3,*]

[1]Research Programs Unit, Molecular Neurology, Biomedicum Helsinki, [2]Department of Pathology and [3]Department of Medical Genetics, Haartman Institute, University of Helsinki, Helsinki, Finland, [4]Molecular Neurogenomics Group, VIB Department of Molecular Genetics and [5]Institute Born-Bunge, University of Antwerp-CDE, Antwerp, Belgium and [6]Division of Child Neurology, Helsinki University Central Hospital, Helsinki, Finland

Received February 7, 2013; Revised and Accepted March 29, 2013

Inherited peripheral neuropathies are a heterogeneous group of disorders that can affect patients of all ages. Children with inherited neuropathy often develop severe disability, but the genetic causes of recessive early-onset axonal neuropathies are not fully known. We have taken a whole-exome sequencing approach to identify causative disease mutations in single patients with early-onset axonal neuropathy. Here, we report compound heterozygous mutations in the *tripartite motif containing 2* (*TRIM2*) gene in a patient with childhood-onset axonal neuropathy, low weight and small muscle mass. We show that the patient fibroblasts are practically devoid of TRIM2, through mRNA and protein instability caused by the mutations. TRIM2 is an E3 ubiquitin ligase that ubiquitinates neurofilament light chain, a component of the intermediate filament in axons. Resembling the findings in our patient's sural nerve biopsy, Trim2-gene trap mice showed axonopathy with accumulations of neurofilaments inside axons. Our results suggest that loss-of-function mutations in *TRIM2* are a cause of axonal neuropathy, which we propose to develop as a consequence of axonal accumulation of neurofilaments, secondary to lack of its ubiquitination by TRIM2.

INTRODUCTION

Charcot–Marie–Tooth disease (CMT) is the most common inherited neuromuscular disorder presenting with progressive neuropathy of the motor and sensory nerves. The clinical phenotypes vary from severe infantile-onset multisystem disorders to mild late-onset isolated peripheral neuropathies (1). CMT is classified as demyelinating type (CMT1) when nerve conduction velocity is decreased and as axonal type (CMT2) when NCV is normal or slightly reduced, although overlapping intermediate phenotypes also exist (2). The inheritance of CMT can follow all Mendelian forms with more than 40 disease genes described to date (3). Although the same disease genes have been found to contribute to both dominant and recessive disease, early-onset CMT is more likely to result from recessively inherited mutations (4).

Disease genes linked to the demyelinating CMT1 phenotypes are expressed predominantly in Schwann cells but more functional heterogeneity is found in axonal CMT2 neuropathies. Axons are remarkably specialized structures that can exceed 1 m in length, which makes them sensitive to derangements in a number of cellular functions such as transport processes and cytoskeletal organization (5). CMT2 disease genes encode proteins with diverse functions, including mitochondrial network regulation, organelle transport, protein synthesis, endocytosis and maintenance of the cytoskeleton (6,7).

Estimated 30–50 disease genes for hereditary neuropathies remain to be identified (8) and especially many of the genetic defects underlying early-onset axonal neuropathy are not known. The CMT genes most often associated with axonal neuropathies in children are *MFN2*, *TRPV4*, *GDAP1* and *NEFL* (4,6). The latter encodes neurofilament light (NF-L) chain, a subunit of the neuron-specific intermediate filament, which is an essential component of the axon's cytoskeleton. Early-onset neuropathy may also be found in the following conditions: spinal muscular atrophies, congenital axonal

*To whom correspondence should be addressed at: Biomedicum Helsinki, r.C520b, Haartmaninkatu 8, 00290 Helsinki, Finland. Tel: +358 919125654; Fax: +358 919125610; Email: henna.tyynismaa@helsinki.fi

neuropathies with central nervous system involvement, giant axonal neuropathy (GAN), mitochondrial DNA depletion syndromes and fatty-acid oxidation disorders (9).

We have taken a whole-exome sequencing approach to identify disease mutations in our patients with early-onset axonal neuropathy. Here, we describe the identification of mutations in *TRIM2* by exome sequencing in a patient with childhood-onset neuropathy with neurofilament disorganization in the peripheral nerves.

RESULTS

Patient with early-onset axonal neuropathy of unknown cause

Our patient is an 18-year-old female, who has been followed up at Children's Hospital in Helsinki University Central Hospital. She was born after an uneventful pregnancy as a second child in a family with no consanguinity. Her birth weight was 3.570 g and the Apgar score was 9. Her early development was normal. At the age of 8 months, she was sent to a pediatrician because of poor growth, but no abnormality was found. Her gross-motor development became slower after the age of 1 year. She started walking without support at the age of 18 months and was sent to our hospital because of muscle hypotonia at the age of 4 years. The investigations revealed a very co-operative and alert girl, who was of slight build and had small muscle mass with generalized muscle hypotonia and atrophy of the small muscles in hands and feet. The deep tendon reflexes were absent, and the Babinski sign was negative. She walked with broad base, and could not walk on heels. Electroneuromyography at the age of 4 years 2 months showed polyneuropathy: in upper extremities, the motor nerve conduction velocities were slow (right median nerve 29 m/s, right ulnar nerve 30 m/s) with increased distal latencies (median nerve 4.4 ms, ulnar nerve 3.3 ms) and low amplitude (median nerve 0.7 mV, ulnar 0.5 mV). The sensory amplitudes were low in upper extremities (right median nerve 43 m/s, amplitude 6 μV), and in lower extremities even the motor responses could not be measured.

The brain MRI was normal, as well as the results of the following laboratory tests: peripheral blood count, serum or blood concentrations of aminotransferase, ammonia, creatine kinase, lactate, pyruvate, carnitine, free fatty acids, cholesterol, triglycerides, vitamins A and E, very long-chained fatty acids and phytanic acid, urine metabolic screening and organic acids.

During the 15 years of follow-up, the audiometric hearing tests and ophthalmologic examinations including pattern-visual evoked potential and visual field studies have remained normal. No sign of cranial nerve involvement has appeared. There is no cardiac involvement; the 24 h EKG registration and cardiac echography were examined at the age of 16 years.

The patient has remained thin, her length is −1 SD, but the weight has gone down between −3.5 and −4 SD, mainly because of small volume of muscle and fat, but the sexual maturation has been normal.

Both feet have been operated on because of cavus deformity. The patient walks using light carbon fiber leg-orthoses. Because of muscle weakness, she cannot carry heavy bags or walk long distances. She writes with a computer, and requires aid to open locks or tight lids. Still, in spite of the considerable muscle weakness and motor disability, the patient is very active and has just graduated from high school.

Neurofilament accumulation in sural nerve biopsy

A sural nerve biopsy was performed at the age of 5 years 1 month according to the histological and electron microscopic techniques described earlier (10). Examination of toluidine blue-stained semi-thin sections revealed a normal fascicular structure, and no specific pathology was observed in epineurium or blood vessels or in the perineurial sheaths. The endoneurium displayed a mild to moderate loss of myelinated fibers, more prominent regarding large myelinated fibers of >7 μm in diameter (Fig. 1A and B). The total density of myelinated fibers (MF) was 8600 MF/mm^2, which is ∼50% of the normal value in this age group. Large MF represented only 24% of all MF, the normal range being 35–45%. Some unspecific degenerative axonal features were observed, but no clear signs of active demyelination, hypertrophy or marked regenerative sprouting were seen. In electron microscopy, some slightly swollen large MF were found, in which the axoplasm revealed prominent neurofilament content compared with microtubule density (Fig. 1C and D). The sural nerve biopsy findings were consistent with an axonal neuropathy devoid of truly specific findings, although some large swollen axons could be seen.

Whole-exome sequencing reveals *TRIM2* mutations

To identify the causative gene defect, we sequenced the exome of our patient. The variant filtering of the exome data was done assuming recessive inheritance. Novel homozygous variants were first inspected, but none with damaging prediction to protein function according to the SIFT tool (http://sift.jcvi.org/) were found. We then proceeded to filter for compound heterozygous mutations. The single-nucleotide variant (SNV) data were filtered as follows: (i) exclusion of homozygous variants; (ii) exclusion of previously known single-nucleotide polymorphisms according to dbSNP (http://www.ncbi.nlm.nih.gov/snp/, accessed May 2012) and 1000 Genomes Project (http://www.1000genomes.org/); (iii) exclusion of variants with a synonymous or nonsynonymous tolerated prediction according to the SIFT prediction. The variant data containing insertions and deletions (indel) were filtered as follows: (i) exclusion of homozygous indel variants; (ii) exclusion of previously known variants according to dbSNP; (iii) exclusion of indel variants that do not locate in exons. Then, the lists of heterozygous SNV and indel variants were combined and filtered for genes with more than one variant. This final step yielded a list of 23 genes with compound heterozygous mutations that were selected for further analysis.

Only one of these genes, *TRIM2* (tripartite motif containing 2), had previously been linked to axonal function (11,12). The first of the identified *TRIM2* variants was a heterozygous missense mutation (c.680A>T, [p.E227V], RefSeq accession number NM_001130067.1). The second variant was a 1 bp deletion leading to a frameshift and a premature stop codon (c.1699delA, [p.K567Rfs7X]). Sanger sequencing confirmed

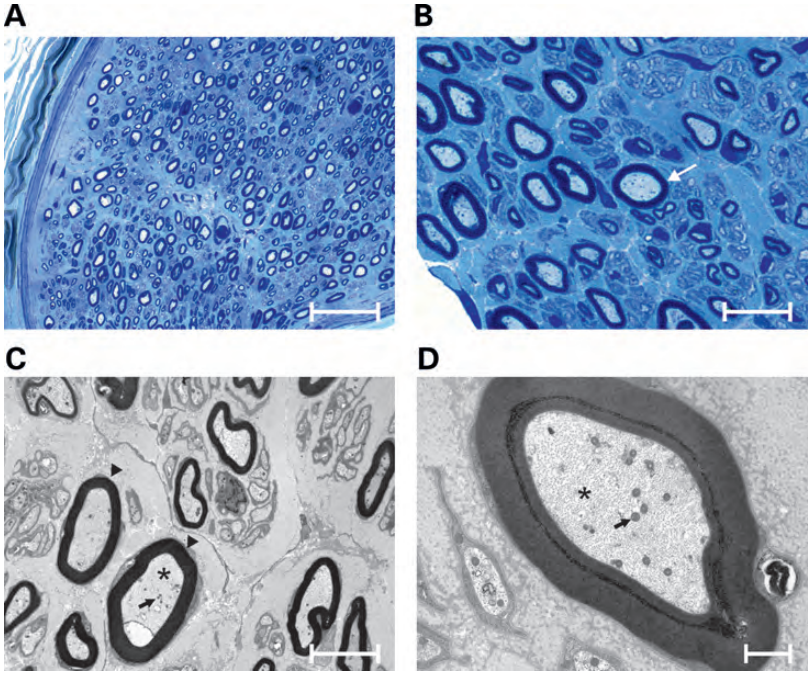

Figure 1. Sural nerve biopsy findings. (**A**) In plastic sections, the density of MF is reduced. Semi-thin toluidine blue-stained plastic section, original magnification ×400; bar = 30 μm. (**B**) At higher magnification, the toluidine blue-stained semi-thin section reveals MF swelling (arrow), original magnification ×1000; bar = 10 μm. (**C**) In electron microscopy, some swollen MF are seen in the center (arrowheads). In the axoplasm, the relative density of neurofilaments is increased (asterisk) compared with microtubules (arrow). Electron micrograph, original magnification ×5300; bar = 5 μm. (**D**) A higher magnification micrograph shows a swollen MF containing neurofilaments (asterisk) at high density compared with microtubules (arrow); original magnification ×20 000; bar = 1 μm.

that the proband carried both mutations, whereas her father was heterozygous for c.1699delA and her mother for c.A680T (Fig. 2A), and her healthy brother did not carry either mutation. Neither mutation was found in 366 Finnish control chromosomes by solid-phase minisequencing (13).

TRIM2 instability in patient fibroblasts

To study the effects of the *TRIM2* mutations, we obtained cultured fibroblasts from a skin biopsy of the patient. Sanger sequencing of the cDNA derived from these cells showed homozygosity for the c.A680T mutation while the c.1699delA variant was undetectable, suggesting degradation of the mRNA containing the 1 bp deletion through nonsense-mediated decay (NMD) (Fig. 2A). Indeed, cycloheximide (CHX) treatment inhibiting NMD restored the cDNA heterozygosity for both of the mutations (Fig. 2A). Allele-specific quantitative PCR showed that, in patient cells, the proportion of the cDNA derived from the c.1699delA allele, containing wild-type c.680A, was 7% of total TRIM2 cDNA, which increased to 33% with 24 h of CHX treatment (Fig. 2B). Together, these results showed that the c.1699delA mRNA was subject to degradation by NMD, suggesting that the TRIM2 protein in patient cells originated almost completely from the c.680T mutant allele that encodes the p.E227V protein.

Unexpectedly, western blots with polyclonal *TRIM2* antibody (Sigma SAB4200206, amino acids 292–310) showed that the TRIM2 protein was nearly undetectable in patient fibroblast lysates (Fig. 3A). Accurate densitometric quantification was problematic to perform because of the low TRIM2 signal in patient cells, but resulted, on average, in ∼13% of residual TRIM2 compared with control cells, suggesting that the protein containing the p.E227V variant was largely unstable (Fig. 3B).

TRIM2 is a RING finger protein containing an RBCC domain [RING finger, B-box zinc finger, coiled-coil (CC)] and a beta-propeller (NHL) domain (14) (Fig. 3C), and it functions as an E3 ubiquitin ligase (11). The p.E227V change affects a highly conserved amino acid (Fig. 3E) and locates to the CC domain of TRIM2 (Fig. 3C). The predicted CC region in RBCC proteins is typically approximately 100 residues long and broken up into two or three separate CC motifs that are thought to function in homo interactions, in complex formation or in determining subcellular localization (15,16). The Paircoil2 software (17) predicted that the TRIM2 CC domain is split into two CC motifs (predicted amino acid positions 183–222 and 256–289) separated by an intercoil region (predicted amino acid positions 223–255) (Fig. 3D). CC motifs are known to tolerate amino acid variation as long as the requirement of heptad repeats with hydrophobic amino acids at specific positions is met. Accordingly, the predicted CC motifs in TRIM2 contain several non-conserved residues (Fig. 3D). The p.E227 residue, however, is positioned in a very highly conserved stretch of 23 amino acids (amino acid positions 211–233) at the junction of the first CC motif and the intercoil region (Fig. 3D).

The low level of TRIM2 protein in patient fibroblasts suggested that the p.E227V mutant protein was unstable. To further assess this possibility, we transfected HEK cells with expression vectors for the wild-type and p.E227V mutant TRIM2 and subjected those to a time course CHX stability assay. The result suggested reduced stability for the mutant

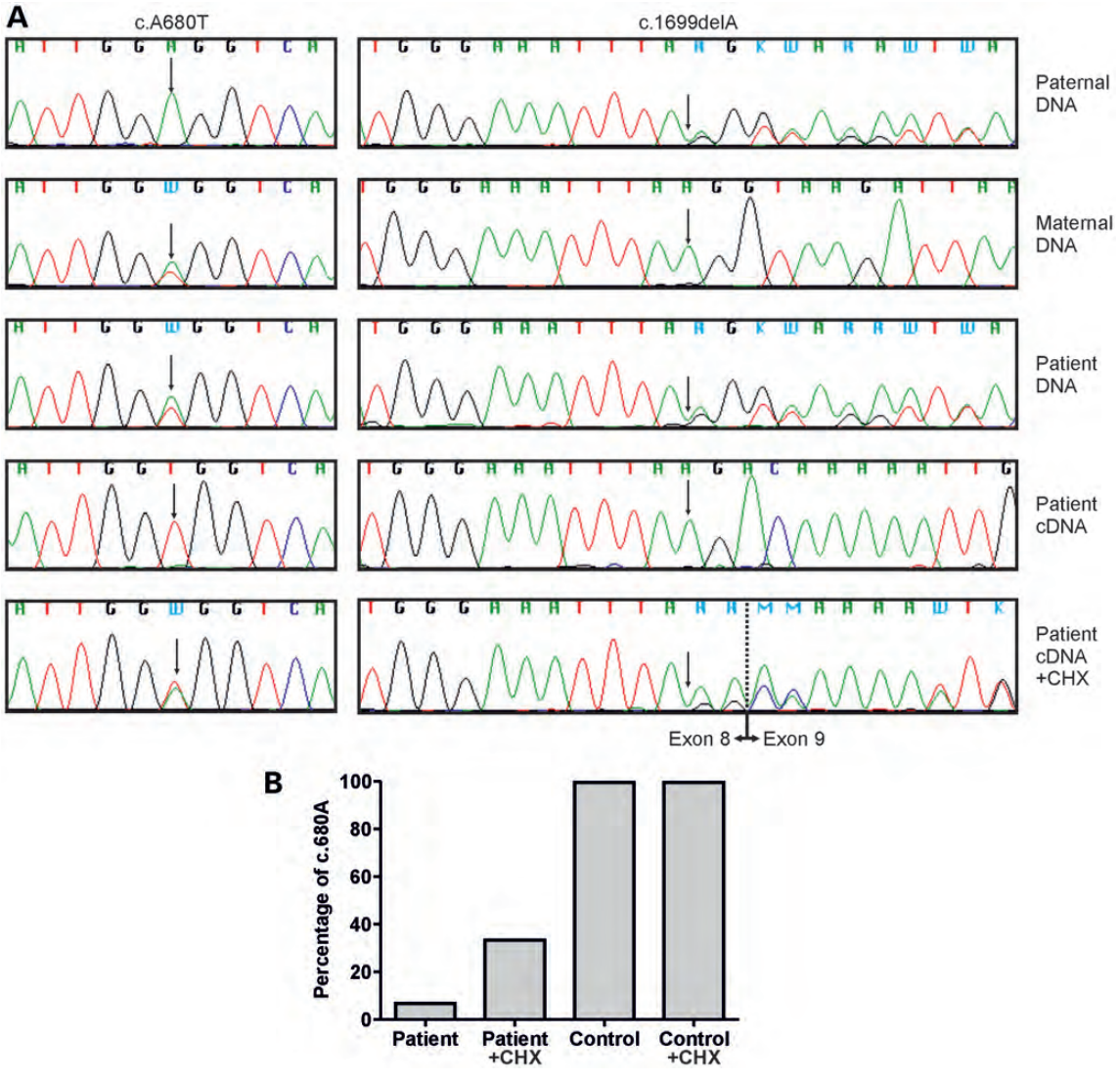

Figure 2. *TRIM2* sequencing. (**A**) Sanger sequencing shows that the patient's genomic DNA is compound heterozygous for the *TRIM2* c.A680T and c.1699delA mutations, whereas her father is heterozygous for the latter and her mother for the former. Sequencing of patient cDNA from fibroblasts detects the c.A680T mutation in the homozygous state, whereas c.1699delA is undetectable. Inhibition of NMD with CHX prevents the degradation of the c.1699delA mRNA as detected by Sanger sequencing of cDNA from CHX-treated patient cells. (**B**) Allele-specific quantitative PCR of patient and control cDNA from untreated and CHX-treated fibroblasts shows that the residual amount of the c.1699delA mRNA (detected as wild-type for c.680A) was 7% in untreated patient cells, increasing to 33% after CHX treatment.

protein in comparison with the wild-type TRIM2 also in the overexpression conditions (Fig. 4).

To determine whether the lack of TRIM2 in patient cells resulted from a post-translational degradation by the proteasome, we treated patient and control fibroblasts with the proteasome inhibitor MG132. This treatment did not significantly increase TRIM2 protein levels in patient cells (Fig. 3F), suggesting that the mutant TRIM2 is degraded by another pathway than the proteasome.

TRIM2 deficiency does not affect intermediate filament architecture in fibroblasts

NF-L is one of the ubiquitination targets of TRIM2 (11). *TRIM2* has a ubiquitous mRNA expression in human tissues (Fig. 5A), which led us to investigate whether TRIM2-deficiency influences the architecture of intermediate filaments other than the neurofilament. In another disease of the peripheral nervous system showing neurofilament accumulation, GAN, the patients have a defect in gigaxonin protein that mediates the ubiquitination of intermediate filaments including neurofilaments, leading to an early-onset progressive disease with giant axonal distension (18,19). Cultured fibroblasts of patients with *GAN* mutations contain cytoplasmic vimentin inclusions (20). To test whether TRIM2 has a broader role in intermediate filament maintenance outside the axons, we stained the patient fibroblasts using anti-vimentin antibody. Our stainings showed that on the contrary to GAN patients, TRIM2-deficient patient fibroblasts had normal vimentin architecture (Fig. 5B).

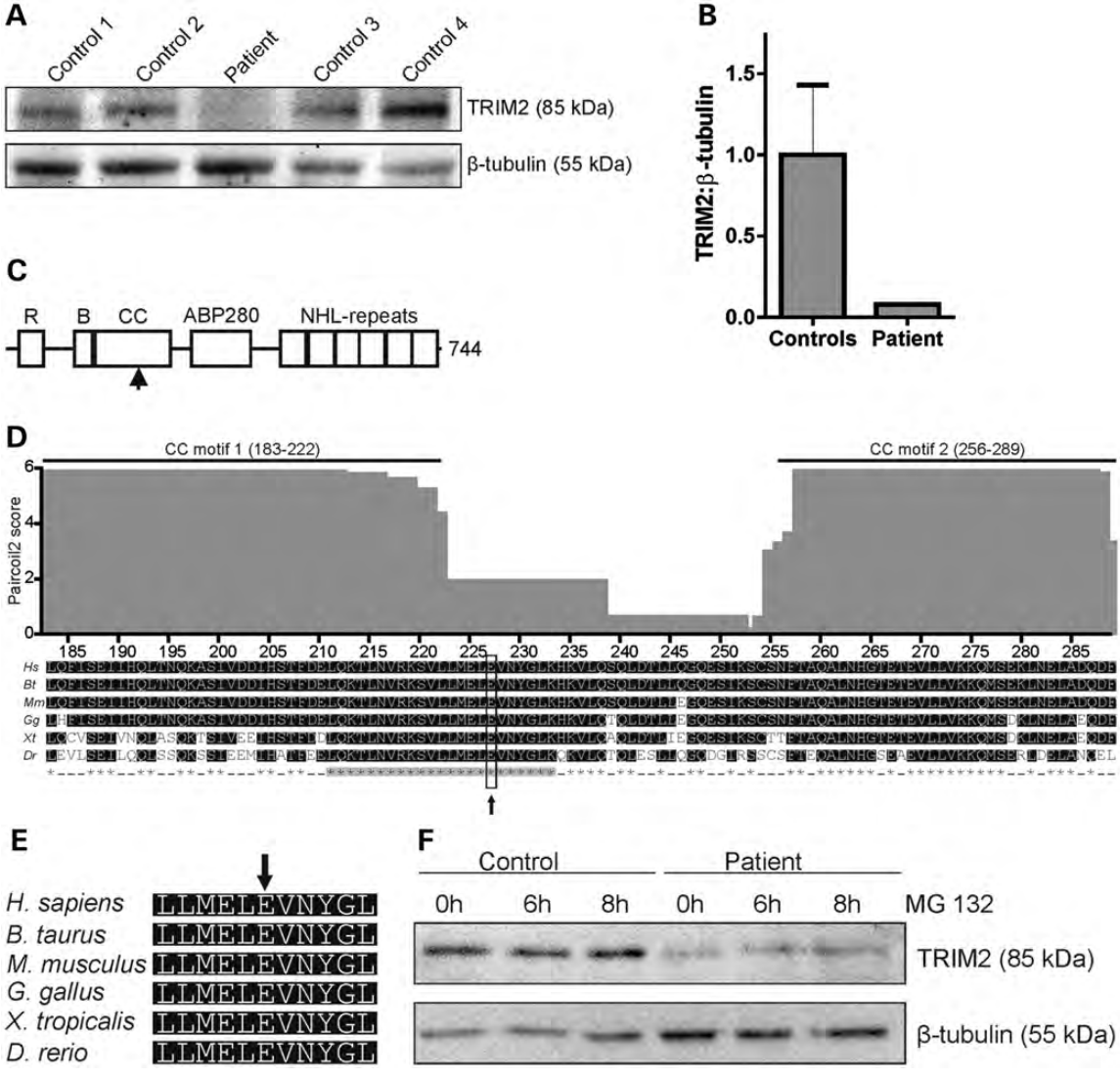

Figure 3. TRIM2 deficiency in patient fibroblasts. (**A**) Western blots of total protein extracts of control and patient fibroblasts. Control cells show a clear TRIM2 signal of ~85 kDa, whereas it is nearly undetectable in patient cells. (**B**) Densitometric quantification of TRIM2 protein (controls $n = 3$); the error bar indicates SEM. The residual TRIM2 level was on average 13.4% ± 3.4% (SEM) in three independent experiments, each of which compared the patient TRIM2 level with the average TRIM2 level of three unrelated control fibroblast lines. (**C**) The TRIM2 primary structure is schematically shown with p.E227 marked with an arrow. (**D**) The p.E227V missense change affects a highly conserved residue in the CC domain of TRIM2. Paircoil2 predicted that the CC domain of TRIM2 contains two CC motifs (amino acid positions 183–222 and 256–289) separated by an intercoil region that partially includes a highly conserved stretch of amino acids (highlighted in gray). (**E**) Alignments of E227 (arrow) and adjacent amino acids are shown enlarged. (**F**) Proteasome inhibition had no significant effect on TRIM2 protein levels. Western blots of total protein extracts of control and patient fibroblasts following treatment with 10 μM of the proteasome inhibitor MG132 for 0, 6 or 8 h. The patient samples were overloaded to increase the detectability of the TRIM2 signal.

TRIM2 mutations are a rare cause of early-onset axonal neuropathy

To determine the prevalence of *TRIM2* mutations in patients with neuropathy phenotypes, we proceeded to investigate a heterogeneous international cohort of 87 early-onset patients for mutations in *TRIM2* by sequencing the coding exons. In 66 patients, the clinical diagnosis was axonal CMT, in 9 demyelinating CMT and in 12 intermediate CMT. The age at onset in 33 probands was between 1 and 5 years; in the remaining patients, it was after the age of 5, but still within the first decade of life. Ten patients had a CMT plus syndrome associated with optic atrophy, deafness, vocal cord paralysis or ataxia. No putative mutations were identified in any of the screened patients, indicating that *TRIM2* has a low mutation frequency and is thus a rare cause of early-onset axonal CMT.

DISCUSSION

The identification of the causative disease mutations in single patients using exome sequencing is a challenging task despite the improvements of the bioinformatics processes and the accumulation of natural variation data in publicly available databases. Although all individuals carry multiple private variants, most of them are neutral and it is less common to find two

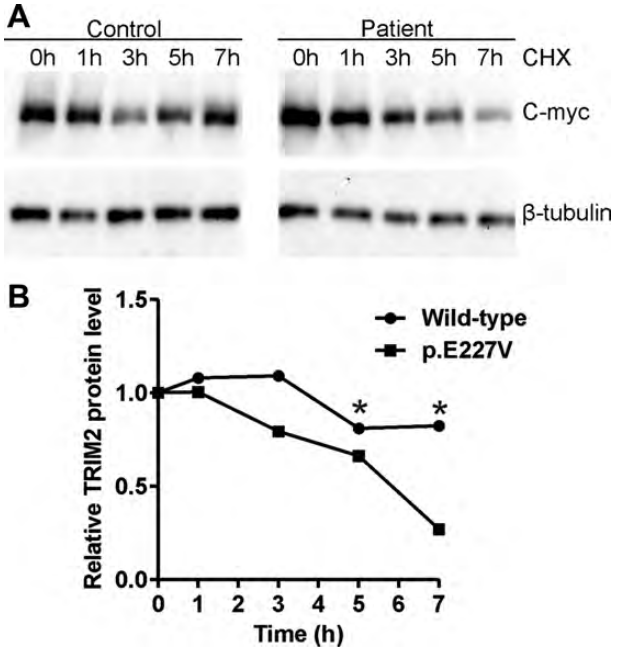

Figure 4. CHX time course of TRIM2 stability. (**A**) HEK cells were transfected with myc-tagged TRIM2 constructs containing wild-type cDNA or the p.E227V mutant. CHX was added to both, and a time course from 0 to 7 h was performed. Cell lysates were analyzed by immunoblot using antibodies to c-myc and beta-tubulin. (**B**) Densitometric quantification of TRIM2 protein in relation to beta-tubulin during the time course shows reduced stability for the p.E227V mutant. The average of three independent experiments is shown. The asterisk indicates statistical significance of $P < 0.05$.

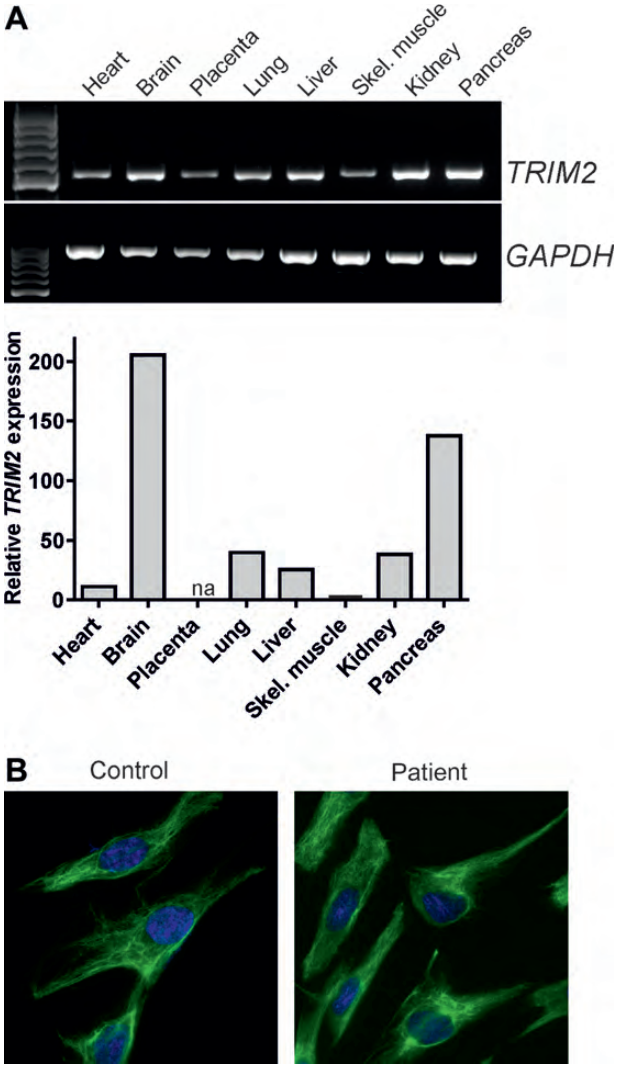

Figure 5. *TRIM2* tissue expression and vimentin organization in patient fibroblasts. (**A**) PCR of *TRIM2* was performed on a cDNA library of the indicated tissues. *GAPDH* was used as the loading control. Quantifications of the relative tissue expression of *TRIM2* by quantitative PCR are shown in the lower panel. The *TRIM2* signal was normalized to the *GAPDH* for the respective tissues, and the data are presented relative to the skeletal muscle expression level. In placenta, *TRIM2* could not be reliably detected by quantitative PCR (na, not available). (**B**) Immunostaining for vimentin (green) together with DAPI (blue) showed normal organization of the vimentin fibers in control and patient fibroblasts (63× oil immersion objective). At least 50 cells were analyzed in each case; shown are representative examples.

private mutations with predicted damaging effect in the same gene. This was the basis behind the identification of compound heterozygous *TRIM2* mutations in the patient studied here. Neither variant is listed in sequencing databases containing data from thousands of samples, nor did we find them in the controls from our population. Importantly, we show that the mRNA containing the 1 bp deletion is degraded, and that the p.E227V variant protein is largely unstable. Thus, the patient cells show a significant deficiency of TRIM2, which has not been previously described in humans, demonstrating that both of the identified mutations are indeed deleterious.

The next crucial question was whether TRIM2 deficiency can cause the early-onset axonal neuropathy phenotype in our patient. Strong indication for this comes from the gene trap mouse model of *Trim2* ($TRIM2^{GT}$) that had a residual of ~5% of wild-type *Trim2* mRNA and presented with axonopathy followed by progressive neurodegeneration (11). The mouse axons showed neurofilament accumulation, which was suggested to result from deficient ubiquitination and thus inefficient degradation of the NF-L subunit of neurofilaments, a substrate of TRIM2-mediated ubiquitination (11). Consistently, the sural nerve biopsy of our patient showed progressive axonal degeneration with accumulation of neurofilaments. The $TRIM2^{GT}$ mice had central nervous system involvement, whereas the symptoms in our patient were restricted to the peripheral nervous system. This discrepancy may be explained by differences in the regulation of NF-L ubiquitination between the two species. Our efforts to precisely quantify the TRIM2 levels in patient fibroblasts were hampered by the very low levels of detectable protein, but ~10% of TRIM2 was present in the patient cells. The residual protein level in axons may well differ from that in fibroblasts. Nevertheless, the different residual levels of TRIM2 in the $TRIM2^{GT}$ mouse and in our patient tissues may explain the broader phenotype of the mice. We conclude that TRIM2 deficiency is associated with neurofilament accumulation and axonal degeneration in humans as in mice.

The E227 amino acid is located in a very highly conserved part of the CC domain of TRIM2. The high degree of conservation suggests that this region has an important function in,

for example, mediating specific protein interactions. We hypothesize that the loss of ability to self-interact or to bind to other key interacting proteins mediates the instability of the mutant TRIM2. We also found that proteasome inhibition in patient cells did not increase TRIM2 levels, suggesting that the mutant TRIM2 may be degraded through pathways other than the proteasome, by lysosomal and autophagic degradation (21).

Ubiquitination of a protein is an important modifier of its localization, function or degradation. TRIM2 belongs to the family of TRIM/RBCC proteins that function as E3 ubiquitin ligases by binding to both ubiquitin E2-conjugating enzymes and target proteins to facilitate the selective ubiquitination of the target (22). TRIM2 has been proposed a role in axon specification during development (12). Other TRIM proteins are involved in a broad range of cellular processes (15), which explains their association with very different Mendelian genetic diseases. For instance, *TRIM37* is mutated in mulibrey nanism (23), a recessive disorder that targets mesodermal tissues, and a translocation of the TRIM gene *PML* has been identified in promyelocytic leukemia (24). Deficient ubiquitination by other RING finger proteins also impairs ubiquitin-mediated degradation, such as Parkin mutations in juvenile Parkinson's disease, leading to toxic intraneuronal inclusions (25).

NF-L has been described as an important target of ubiquitination by TRIM2 (11). Together with subunits medium (NF-M) and heavy (NF-H), NF-L forms neurofilament, which is a dynamic controller of axon diameter. Neurofilament recycling is important for axon maintenance, indicated by the many neurological disorders that result from excessive neurofilaments in axons. Importantly, mutations in *NEFL* (encoding NF-L) cause CMT2 by impairing neurofilament transport leading to its accumulation within neurons (26). *NEFH* (encoding NF-H) mutations are associated with amyotrophic lateral sclerosis susceptibility (27). Accumulation of neurofilaments is a well-known phenomenon also in other neurodegenerative disorders, such as Alzheimer's disease (26). Furthermore, patients with GAN show neurofilament accumulation because of its deficient ubiquitination (18,19). The defect in the patients with GAN is not restricted to the intermediate filaments in axons because patient fibroblasts have vimentin inclusions (20). TRIM2 is also expressed ubiquitously, but we did not find indications of vimentin disorganization in the fibroblasts of our patient. Other substrates than NF-L are, however, likely to exist for TRIM2, and phosphorylated Bcl2-interacting mediator of cell death has been reported as such target (28). Our patient was markedly underweight and had low adipose tissue content despite exhaustive dietary measures; hence, novel substrates for TRIM2 in nutrient absorption or metabolism are conceivable.

CMT diseases are clinically and genetically heterogeneous with a large number of underlying disease genes. Genetic defects leading to early-onset recessive axonal neuropathies are not well known. We examined the overall contribution of *TRIM2* mutations to CMT with an onset in the first decade of life by screening a large patient cohort for mutations. The result showed that coding region mutations in *TRIM2* are a rare cause of early-onset CMT neuropathy. Patients with higher ages of onset and/or with a different clinical course of neuropathy were not investigated for *TRIM2* mutations in this study. Common to the heterogeneous CMT disease, defects in the same gene may cause highly variable clinical outcomes.

In conclusion, our study has identified TRIM2 deficiency in a patient with early-onset severe CMT2. Exome sequencing is a powerful technique to provide molecular diagnosis in individual patients and can bring important knowledge on disease etiology. Our results highlight the importance of inefficient neurofilament degradation as a pathogenic mechanism in axonal neuropathy.

MATERIALS AND METHODS

Patient study information

This study was carried out in accordance with the Declaration of Helsinki. All involved subjects gave written informed consent, and the study was approved by the ethics board of the Helsinki University Central Hospital.

DNA sequencing

Target-enrichment was done using NimbleGen Sequence Capture 2.1M Human Exome v2.0 array and sequencing with the Illumina Genome Analyzer-IIx platform. 2 × 82 paired-end reads were aligned to the hg19 assembly, using the variant calling pipeline of the Finnish Institute of Molecular Medicine (29). The procedure yielded 49× mean coverage of target bases. The coding exons of *TRIM2* were bidirectionally Sanger-sequenced using ABI3730xl DNA Analyzer (Applied Biosystems) and analyzed with the SeqMan™ II software (DNASTAR, Inc.). Primer sequences are available on request. Solid-phase minisequencing was performed as described (13).

cDNA synthesis and sequencing

Total RNA was isolated from semi-confluent 10 cm plates of fibroblasts using the NucleoSpin RNA II Kit (Macherey-Nagel). After this, cDNA was synthetized with random priming using the M-MLV reverse transcriptase (Promega). For the sequencing of the c.A680T mutation in *TRIM2*, cDNA was PCR-amplified with Finnzymes Phusion DNA polymerase (Thermo Scientific) using the primers ACCCCACAGTTCCACTCAAG and TTAAGATCGTCCCGAGGTTG. Cycling conditions were 98°C for 30 s, followed by 30 cycles of 98° for 10 s, 58°C for 30 s and 72°C for 2 min. For the sequencing of the c.1699delA mutation, the primers TCTTCAGGGGGTAGCTGCAT and CCTTCCTGATTAAACACCTTGACA were used. PCR amplification was followed by bidirectional Sanger sequencing as described earlier.

Allele-specific quantitative PCR

DyNAmo Flash SYBR Green QPCR Kit (Thermo Scientific) was used for the quantitative PCR according to the manufacturer's instructions. Reactions were run on a Bio-Rad C1000 Touch Thermal Cycler. For allele-specific QPCR of *TRIM2* cDNA, we used the forward primer ACCCCACAGTTCCACTCAAG together with the reverse primer TTTGAGGCCATAGTTGACCT for specific amplification of the c.680A or TTTGAGGCCATAGTTGACCA for c.680T, respectively. *GAPDH* cDNA was amplified as a loading control using the primers CGCTCTCTG CTCCTCCTGTT and CCATGGTGTCTGAGCGATGT. CHX

treatment of 100 ng/μl (Sigma C7698) for 24 h was used to inhibit NMD.

Western blotting

Primary fibroblasts were lysed in RIPA buffer (1% NP40, 0.05% sodium deoxycholate and 0.1% sodium dodecyl sulfate in phosphate buffered saline), followed by immunoblotting with anti-TRIM2 (Sigma-Aldrich SAB4200206) and anti-tubulin (Cell Signaling #2146) antibodies. Bands were visualized with the ECL Prime Detection Reagent (GE Healthcare), imaged with a Chemidoc XRS+ Molecular Imager (Bio-Rad) and quantified with the ImageQuant TL software (GE Healthcare).

CHX stability assay

The construct in pCS2 carrying c-myc-tagged mouse WT *Trim2* cDNA was a kind gift from Dr Martin Balastik (11). Site-directed mutagenesis was used to introduce the nucleotide change corresponding to p.E227V, using primers GCTCATGGAGTTGGTGGTCAACTATGGTC and GACCATAGTTGACCACCAACTCCATGAGC. HEK cells were transfected using the jetPRIME transfection reagent (Polyplus) according to the manufacturer's instruction. Twelve hours after transfection, media were supplemented with 100 ng/μl of CHX, and the cells were collected at time points 0, 1, 3, 5 and 7 h. The levels of TRIM2 protein were measured using western blot with anti-c-myc antibody (Roche #11–667149001) and normalized to tubulin as described earlier.

Tissue mRNA expression

PCR was performed on a Human MTC Panel I cDNA library (Clontech) according to the manufacturer's instructions. For *GAPDH* cDNA, the primers were supplied with the kit and for *TRIM2* cDNA, the primers TCTTCAGGGGGTAGCTGCAT and CCTTCCTGATTAAACACCTTGACA were used. QPCR was done from the same cDNA library as described under allele-specific QPCR using the following primers: TTTGAGGCCATAGTTGACCA and GAAATTGTTCTGGAGCGCGG for *TRIM2* cDNA and primers CGCTCTCTGCTCCTCCTGTT and CCATGGTGTCTGAGCGATGT for *GAPDH* cDNA.

Immunocytochemistry

Primary fibroblasts were fixed in paraformaldehyde, permeabilized with Triton X and stained with anti-vimentin antibody (Cell Signaling #5741) and DAPI. Imaging was done with an Axioplan 2 fluoresence microscope (Zeiss) and the AxioVision 4.8.1.0 software.

ACKNOWLEDGEMENTS

The authors would like to thank the patient and her family for participation in the study. Riitta Lehtinen and Annika Stormbom are thanked for technical help. Jukka Kallijärvi and Brendan Battersby are thanked for discussions and expertise and Martin Balastik for plasmids. We also acknowledge the exome capture, sequencing and variant-calling pipeline analysis performed by the Institute for Molecular Medicine Finland (FIMM), Technology Centre and University of Helsinki.

Conflict of Interest statement. None declared.

FUNDING

This work was supported by the Sigrid Jusélius Foundation; the Academy of Finland; the University of Helsinki; Fund for Scientific Research-Flanders (FWO, grant G054313N); the Methusalem Excellence Grant of the Flemish Government; and the Association Belge Contre les Maladies Neuromusculaires (ABMM).

REFERENCES

1. Szigeti, K. and Lupski, J.R. (2009) Charcot-Marie-Tooth disease. *Eur. J. Hum. Genet.*, **17**, 703–710.
2. Nicholson, G. and Myers, S. (2006) Intermediate forms of Charcot-Marie-Tooth neuropathy: a review. *Neuromolecular Med.*, **8**, 123–130.
3. Patzko, A. and Shy, M.E. (2011) Update on Charcot-Marie-Tooth disease. *Curr. Neurol. Neurosci. Rep.*, **11**, 78–88.
4. Wilmshurst, J.M. and Ouvrier, R. (2011) Hereditary peripheral neuropathies of childhood: an overview for clinicians. *Neuromuscul. Disord.*, **21**, 763–775.
5. Niemann, A., Berger, P. and Suter, U. (2006) Pathomechanisms of mutant proteins in Charcot-Marie-Tooth disease. *Neuromolecular Med.*, **8**, 217–242.
6. Baets, J., Deconinck, T., De Vriendt, E., Zimon, M., Yperzeele, L., Van Hoorenbeeck, K., Peeters, K., Spiegel, R., Parman, Y., Ceulemans, B. *et al.* (2011) Genetic spectrum of hereditary neuropathies with onset in the first year of life. *Brain*, **134**, 2664–2676.
7. Gentil, B.J. and Cooper, L. (2012) Molecular basis of axonal dysfunction and traffic impairments in CMT. *Brain Res. Bull.*, **88**, 444–453.
8. Braathen, G.J., Sand, J.C., Lobato, A., Hoyer, H. and Russell, M.B. (2011) Genetic epidemiology of Charcot-Marie-Tooth in the general population. *Eur. J. Neurol.*, **18**, 39–48.
9. Yiu, E.M. and Ryan, M.M. (2012) Genetic axonal neuropathies and neuronopathies of pre-natal and infantile onset. *J. Peripher. Nerv. Syst.*, **17**, 285–300.
10. Koskinen, T., Sainio, K., Rapola, J., Pihko, H. and Paetau, A. (1994) Sensory neuropathy in infantile onset spinocerebellar ataxia (IOSCA). *Muscle Nerve*, **17**, 509–515.
11. Balastik, M., Ferraguti, F., Pires-da Silva, A., Lee, T.H., Alvarez-Bolado, G., Lu, K.P. and Gruss, P. (2008) Deficiency in ubiquitin ligase TRIM2 causes accumulation of neurofilament light chain and neurodegeneration. *Proc. Natl Acad. Sci. USA*, **105**, 12016–12021.
12. Khazaei, M.R., Bunk, E.C., Hillje, A.L., Jahn, H.M., Riegler, E.M., Knoblich, J.A., Young, P. and Schwamborn, J.C. (2011) The E3-ubiquitin ligase TRIM2 regulates neuronal polarization. *J. Neurochem.*, **117**, 29–37.
13. Suomalainen, A. and Syvanen, A.C. (2003) Analysis of nucleotide sequence variations by solid-phase minisequencing. *Methods Mol. Biol.*, **226**, 361–366.
14. Ohkawa, N., Kokura, K., Matsu-Ura, T., Obinata, T., Konishi, Y. and Tamura, T.A. (2001) Molecular cloning and characterization of neural activity-related RING finger protein (NARF): a new member of the RBCC family is a candidate for the partner of myosin V. *J. Neurochem.*, **78**, 75–87.
15. Meroni, G. and Diez-Roux, G. (2005) TRIM/RBCC, a novel class of 'single protein RING finger' E3 ubiquitin ligases. *Bioessays*, **27**, 1147–1157.
16. Reymond, A., Meroni, G., Fantozzi, A., Merla, G., Cairo, S., Luzi, L., Riganelli, D., Zanaria, E., Messali, S., Cainarca, S. *et al.* (2001) The tripartite motif family identifies cell compartments. *EMBO J.*, **20**, 2140–2151.

17. McDonnell, A.V., Jiang, T., Keating, A.E. and Berger, B. (2006) Paircoil2: improved prediction of coiled coils from sequence. *Bioinformatics*, **22**, 356–358.
18. Bomont, P., Cavalier, L., Blondeau, F., Ben Hamida, C., Belal, S., Tazir, M., Demir, E., Topaloglu, H., Korinthenberg, R., Tuysuz, B. *et al.* (2000) The gene encoding gigaxonin, a new member of the cytoskeletal BTB/kelch repeat family, is mutated in giant axonal neuropathy. *Nat. Genet.*, **26**, 370–374.
19. Kuhlenbaumer, G., Timmerman, V. and Bomont, P. (1993) Giant axonal neuropathy. In Pagon, R.A., Bird, T.D., Dolan, C.R., Stephens, K. and Adam, M.P (eds), *GeneReviews*. University of Washington, Seattle, WA.
20. Pena, S.D., Opas, M., Turksen, K., Kalnins, V.I. and Carpenter, S. (1983) Immunocytochemical studies of intermediate filament aggregates and their relationship to microtubules in cultured skin fibroblasts from patients with giant axonal neuropathy. *Eur. J. Cell Biol.*, **31**, 227–234.
21. Clague, M.J. and Urbe, S. (2010) Ubiquitin: same molecule, different degradation pathways. *Cell*, **143**, 682–685.
22. Dennissen, F.J., Kholod, N. and van Leeuwen, F.W. (2012) The ubiquitin proteasome system in neurodegenerative diseases: culprit, accomplice or victim? *Prog. Neurobiol.*, **96**, 190–207.
23. Avela, K., Lipsanen-Nyman, M., Idanheimo, N., Seemanova, E., Rosengren, S., Makela, T.P., Perheentupa, J., Chapelle, A.D. and Lehesjoki, A.E. (2000) Gene encoding a new RING-B-box-coiled-coil protein is mutated in mulibrey nanism. *Nat. Genet.*, **25**, 298–301.
24. de The, H., Lavau, C., Marchio, A., Chomienne, C., Degos, L. and Dejean, A. (1991) The PML-RAR alpha fusion mRNA generated by the t(15;17) translocation in acute promyelocytic leukemia encodes a functionally altered RAR. *Cell*, **66**, 675–684.
25. Kitada, T., Asakawa, S., Hattori, N., Matsumine, H., Yamamura, Y., Minoshima, S., Yokochi, M., Mizuno, Y. and Shimizu, N. (1998) Mutations in the parkin gene cause autosomal recessive juvenile parkinsonism. *Nature*, **392**, 605–608.
26. Perrot, R., Berges, R., Bocquet, A. and Eyer, J. (2008) Review of the multiple aspects of neurofilament functions, and their possible contribution to neurodegeneration. *Mol. Neurobiol.*, **38**, 27–65.
27. Figlewicz, D.A., Krizus, A., Martinoli, M.G., Meininger, V., Dib, M., Rouleau, G.A. and Julien, J.P. (1994) Variants of the heavy neurofilament subunit are associated with the development of amyotrophic lateral sclerosis. *Hum. Mol. Genet.*, **3**, 1757–1761.
28. Thompson, S., Pearson, A.N., Ashley, M.D., Jessick, V., Murphy, B.M., Gafken, P., Henshall, D.C., Morris, K.T., Simon, R.P. and Meller, R. (2011) Identification of a novel bcl-2-interacting mediator of cell death (bim) E3 ligase, tripartite motif-containing protein 2 (TRIM2), and its role in rapid ischemic tolerance-induced neuroprotection. *J. Biol. Chem.*, **286**, 19331–19339.
29. Sulonen, A.M., Ellonen, P., Almusa, H., Lepisto, M., Eldfors, S., Hannula, S., Miettinen, T., Tyynismaa, H., Salo, P., Heckman, C. *et al.*. (2011) Comparison of solution-based exome capture methods for next generation sequencing. *Genome Biol.*, **12**, R94.